PAN
POLISH ACADEMY OF SCIENCES

Opto-Electronics Review

journal homepage: http://journals.pan.pl/opelre

Simple three-stage frequency-stabilized diode laser system using injection-locking and tapered amplifier

Jerzy Szonert*, Małgorzata Głódź, Krzysztof Kowalski

Institute of Physics, Polish Academy of Sciences, al. Lotników 32/46, 02-668 Warsaw, Poland

Article info

Article history:
Received 2 Aug. 2021
Received in revised form 10 Dec. 2021
Accepted 18 Dec. 2021
Available on-line 28 Feb. 2022

Keywords:
Diode laser; optical injection-locking; master oscillator power amplifier; optical limiting amplifier; tapered amplifier.

Abstract

We developed a three-stage, amplifying, tunable diode laser system that comprises a master laser in a Littrow configuration, frequency-stabilized by dichroic atomic vapour laser lock, acousto-optic frequency shifter, injection-locked slave laser, and tapered amplifier. The slave amplifies the injected frequency-shifted master beam while suppressing (within 0.5%) the strong dependence of its intensity on the acousto-optic frequency shifter carrier frequency, thus acting as a strongly saturated optical limiting amplifier with constant output power. The resulting beam is then amplified in a tapered amplifier. The system provides an output power above 700 mW at a wavelength of 780 nm, with a time-averaged linewidth of 0.6 MHz, and a frequency drift below 2 MHz/h. Dichroic atomic vapour laser lock enables frequency stabilization in the range of 400 MHz around D2 lines of rubidium. The mode-hop-free tuning range amounts to 2 GHz. Determined by the acousto-optic frequency shifter model used, the fine-tuning range (precision of few tens kHz) spans 70 MHz. A description of the system was presented and its performance was tested. The basic components have been designed in our laboratory.

1. Introduction

Tunable continuous-wave (CW) frequency-stabilized lasers of narrow linewidth and significant power are required in diverse applications like nonlinear spectroscopy or optical cooling. Diode lasers (DLs) are compact, cost-effective devices available in a wide range of emission wavelengths, from mid-infrared to violet, that since their development in 1962 have undergone enormous technological progress and have become ubiquitous sources of laser radiation in many fields [1]. However, conventional, solitary, free-running, edge-emitting DLs with a narrow waveguide fail to meet the high requirements. Short cavities with low finesse, broad gain profiles and inherent instabilities result in broadband emission, the frequency stability and tuning achieved by temperature and current control are coarse and suffer from mode-hops, while facet damage limits the output power [2, 3]. Some of the basic approaches developed to improve the lasing characteristics of DL sources [mainly related to those based on Fabry-Perot (FP) type DLs] are outlined below.

The extreme sensitivity of DLs to optical feedback is used in extended (external) cavity diode lasers (ECDLs), where cavity length, feedback selectivity and strength are the main factors influencing their performance [4, 5]. Various elements, such as gratings (reflective [6], transmission [7–9], or volume [10–12]), etalons [13], filters of a narrow- [14] or wide- [15] bandwidth or mirrors [16] are used to improve spectral purity and tunability. Other concepts are also applied, such as, e.g., feedback from a high-finesse optical cavity [17], combination of an ECDL and optical cavity [18], or a compact whispering-gallery-mode resonator [19, 20] that can reduce the linewidth to a level of kHz or below. By far, the most common are ECDLs based on reflective gratings in the Littrow [6, 21, 22] or Littman-Metcalf [23, 24] configurations, each of which possesses its own advantages.

Issues related to improving the performance of ECDLs have been widely investigated. Several methods have been

*Corresponding author at: szonj@ifpan.edu.pl

https://doi.org/10.24425/opelre.2022.140146
1896-3757/ Association of Polish Electrical Engineers (SEP) and Polish Academic of Sciences (PAS). Published by PAS

reported to widen the mode-hop-free (MHF) tuning range, such as: optimization of pivot position [24, 25]; adjustment of cavity length or grating offset to match rates of grating rotation and cavity tuning [26]; synchronization of grating position with the bias current (feed-forward tuning) [27, 28]; use of multiple actuators for the matched translation and rotation of grating [28, 29]; control of cavity length by means of a feedback loop based on polarization spectroscopy [30] or on power monitoring [31]. A common approach is to use the DL with an antireflection (AR) coating [32]. However, the MHF range of 80 GHz [27] (or 137 GHz [33]) for the Littrow type laser and over 100 GHz [34] for the Littman-Metcalf type laser was reported for uncoated DLs, when the injection current and the extended cavity length varied synchronously. Other studies include, e.g., optimization of power and spectral properties with a wave-plate inside the cavity [16, 35]; impact of the collimator position on the feedback efficiency and linewidth [36]; or dependence of the linewidth on grating parameters [37, 38]. Thermal, mechanical, acoustic, pressure or current disturbances cause linewidth broadening, frequency drift, and intensity fluctuation [26, 36, 39]. Countermeasures can be classified as passive and active.

For the former, a compact, stable mechanical structure, and careful separation from ambient perturbations are applied [7, 21, 29, 39–42]. An ECDL design with superior passive properties is presented in Ref. 43, while the concept of a compact design micro-integrated tunable ECDL with no moving parts, suitable for precision spectroscopy in space, is demonstrated in Ref. 10. High sensitivity of the optical frequency to the bias current and temperature (of about −3 MHz/μA and −8 MHz/mK, respectively [26, 36, 39]) requires the use of precise controllers. To address special requirements or for budgetary reasons, many groups decide to develop their own current [42, 44–48] and/or temperature [49, 50] devices.

To actively stabilize short- and long-term frequency fluctuation and drift, numerous techniques have been developed that differ in physical mechanisms, performance, sensitivity to external perturbations and complexity [51–54]. In the present study, a dither-free dichroic atomic vapor laser lock (DAVLL) [51, 55, 56] is applied due to simplicity, reliability, and a broadly tunable locking range. (Variants are also known such as: the use of a millimetre-scale vapor cell [57], a Doppler-free scheme [58, 59] or a related Faraday rotation scheme [60].)

Typically, a complete ECDL-based arrangement for high-resolution applications provides a spectrally and spatially pure beam with a linewidth from tens to hundreds of kHz and MHF tunability of up to tens of GHz, but its output power rarely exceeds few tens of mW, partly due to losses in the optics. However, technological progress has allowed generation of even many watts from a single emitter [1]. For broad-area lasers (BALs), the width of the gain region ranges from tens to hundreds of microns, which can be compared to just a few microns in standard narrow-waveguide devices. However, high powers come at the cost of poor spatial (in the direction where the emitter is elongated) and spectral beam quality. The use of tapered gain regions in the so-called tapered lasers (TLs), and closely related tapered amplifiers (TAs), combine the advantages of low power (narrow-waveguide) and high power (broad-waveguide) DLs which results in high power, improved spectral characteristics, as well as nearly diffraction limited beam quality [61]. In more refined systems, various extended cavity configurations combine with BAL [62–64], TL [65, 66] or TA [14, 24, 67], providing in addition to high power tunability reduced linewidth and improved stability. In some implementations, a spectrally narrow, nearly Gaussian beam has been obtained [14, 24].

An effective approach to produce a high-quality, high-power beam is to separate the generation of the spectrally narrow and diffraction limited beam from its amplification. There are three basic schemes that use semiconductor gain devices [68]: (i) resonant amplification by the optical injection-locking (OIL) [69, 70], (ii) double-pass amplification in the BAL (with an AR-coated front facet and seed injected at a small angle [71, 72], and (iii) travelling-wave amplification in the TA (with both facets quality AR-coated) [68, 73–77]. The two latter schemes are known as the master oscillator power amplifier (MOPA).

Experiments with rubidium atoms often require an intense, stabilized, and tunable CW laser source with a narrow linewidth and a wavelength close to resonance. In this article, a DL-based source designed and built in our laboratory is demonstrated, where both the OIL and MOPA approaches, usually used separately, are combined in a three-stage system using the TA as the power booster. The system comprises: (a) low power grating stabilized ECDL (master laser), followed by two amplifying stages applied in series, (b) OIL amplifier (slave laser), and (c) TA power unit. The master laser is stabilized at a selected frequency near the rubidium transition D2. Before entering the OIL amplifier, the beam is frequency tuned by an acousto-optic modulator (AOM) in a double-pass configuration. Diagnostic tools complete the arrangement. The optical layout of all functional subsystems is shown in Fig. 1. The system that generates a beam with a wavelength of 780 nm and an output power of above 700 mW is designed for studying Rb atoms. However, some of the solutions adopted may also prove useful in systems dedicated to other wavelengths or species. Regarding this introduction, there are a detailed description and characteristics of subsequent functional blocks of the system. Some performance tests and measurements are also included. Finally, brief conclusions are given.

2. Overview of the system

2.1. *Master laser*

Our master laser (DL1 in Fig. 1) is an ECDL in the Littrow configuration with a design inspired by Ref. 21 (and advice from Ref. 6). It includes a popular (uncoated), edge-emitting, single-mode DL (Sanyo DL7140-201M, 70 mW), an aspheric collimator (Thorlabs C230TME-B, f = 4.5 mm, NA = 0.55, AR-coated) and a diffraction grating (Thorlabs GR13-1850, 1800 mm^{-1}). DL was selected for its wavelength from a batch of similar copies. Main components of the mounting assembly are machined of brass. (However, other materials may provide better mechanical or thermal properties [21]). DL and lens are fixed in a way allowing the fine positioning and collimation adjustment. The major axis of the elliptical beam is horizontal and its polarization is vertical. The grating, with

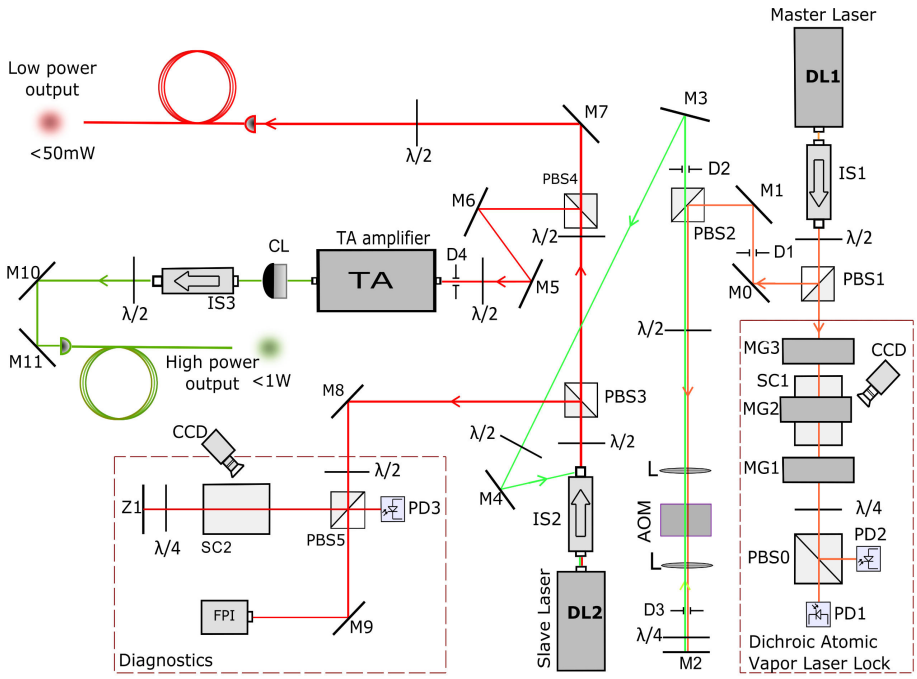

Fig. 1. Optical layout of the amplifying laser system. Description: DL1 master laser, DL2 slave laser, TA tapered amplifier, PBS(0–5) polarizing beam splitter, M(0–11) dielectric mirror, Z1 partially reflecting mirror, λ/2 (λ/4) half- (quarter-) wave plate, PD(1–3) photodiode, IS(1–3) optical isolator, D(1–4) aperture, MG(1–3) permanent toroidal magnet, L lens, CL cylindrical lens, AOM acousto-optical modulator, SC(1–2) Rb vapor cell, FPI spectrum analyser, CCD camera.

vertically positioned groves, is glued to the lever-arm of a flexible hinge (at an angle of incidence of ~45°) that can be precisely tilted horizontally with a fine-pitch screw. Thus, an extended cavity is formed. The first order diffracted beam (~15–20% efficiency) reflects into the DL, while the 0th order is coupled out. A relatively short ~15 mm cavity improves spectral and mechanical stability. The low-voltage piezoelectric transducer (PZT), Piezomechanik PSt 150, placed between the grating arm and the screw tip (secured with a ceramic disc), enables the precise modification of the cavity length. The vertical axis of the grating is tilted with another fine-pitch screw, by flexing the upper surface of the mounting platform ($40\times80\times10$ mm^3) to which the grating mount is rigidly bolted. A small mirror attached to the grating arm compensates the beam deflections [78], however, a small parallel beam walk may still persist. Installed near the DL is a small printed circuit board (PCB) with an anti-spike protection circuit, and a relay that short-circuits the diode when not in use and allows the cables to be disconnected safely. The jumper selects the DL class: cathode- or anode-grounded (our belongs to the former). The PCB also includes a bias-T component enabling a high frequency current modulation (option not used in this application) and is equipped with connectors: two D-sub 9-pin ones and two BNCs, the former are used to connect current and temperature controllers, the latter for the PZT control and current modulation, respectively. The LM35 temperature sensor rests in a small hole near the DL. (However, as we found out later, a better short-term stability (of ±0.1 mK) could be achieved with a NTC 10 kΩ thermistor.) A $40\times40\times4$ mm^3 thermoelectric cooler (TEC) is sandwiched between the mounting platform and the aluminium base ($80\times120\times25$ mm^3), that is fixed to an aluminium heat sink. The ECDL head is covered with a housing to reduce ambient interference. The temperature is stabilized at ~17–20 °C with a homemade precision PID controller [79] (compatible with sensors: LM35, AD590, and NTC 10 kΩ thermistor) with a stability of ±0.2 mK (within 6 h). To run the laser, a high-precision micro-processor controller was designed in our laboratory [80]. It is characterized by a high long-term stability of ±50 nA (within 6 h) and a very low ripple and noise below 50 nA rms (in the range of 10–300 kHz), both values limited by the sensitivity of the available test equipment. It provides a knob adjustable current of 0–350 mA, switchable in four bands. The design includes several safety features: slow start/fast stop (the latter to protect DL in the event of a power failure), adjustable current and voltage limiters, filters, and relay control. It also supplies the PZT with a tunable voltage (range ±15 V) that can be externally modulated. (Note: the frequency response of PZT actuators is usually limited to ~10 kHz, however, due to the combined mass and stiffness of the grating arm, the effective bandwidth is reduced to hundreds of Hz at most. We typically use an asymmetric sawtooth wave at 10–30 Hz. It was found that its falling (return) slope should be longer than 2 ms to avoid mechanical vibrations and the resulting distortions. The controller also enables (i) internal (low frequency, DC to 6 kHz) or external (high frequency, up to 2 GHz) current modulation with a depth of up to 10% of the full-scale range and (ii) current correction synchronous with the PZT voltage (feed-forward compensation).

The ECDL normally runs with a current well above the threshold (~2–3 I_{th}) to generate sufficient power and narrow the linewidth. Based on tuning the laser to a steep slope of a narrow absorption resonance and relating

fluctuations in the transmitted power to optical frequency noise, the linewidth averaged over a few seconds was estimated at 0.6 MHz. (In the preliminary measurement of the optical beat signal between the two similar stabilized ECDLs, a linewidth below 1 MHz was determined.) As no special efforts have been made in the design process, the MHF range is of ~0.5 GHz for the PZT tuning alone. However, synchronous current corrections (with a feed-forward coefficient $\Delta I_{DL}/\Delta V_{PZT} \approx -0.5$ mA/V) allow the range to be extended to ~2 GHz.

The linearly polarized beam is passed through an optical isolator IS1 (Isowave I-80-5M-SD, 60 dB of ~75% transmission) to avoid back reflection and splits on a polarizing beam splitter PBS1 which, together with the half-wave plate, acts as a variable beam divider. The main (reflected) beam has a power of ~12–15 mW, while a weak transmitted beam is used to stabilize the frequency.

2.2. Frequency stabilization system

Locking the single-frequency laser to a narrow resonance is a prerequisite for all high-precision experiments. In the DAVLL scheme, a magnetic field splits the Doppler-broadened lines and a signal of the induced circular dichroism is used as an error signal [55, 56, 81, 82]. The scheme of a circular polarimeter is shown in Fig. 1. A weak ~0.1 mW linearly polarized beam from the ECDL is passed through a homemade cylindrical glass cell of SC1 (6 cm long, 3 cm in diameter) filled with natural Rb vapor at room temperature. Three identical toroidal permanent magnets, with an outer (inner) diameter of 15 (12) cm, thickness of 1.5 cm, and spacing of 4 cm, surround the cell and produce a reasonably uniform (~5%) axial magnetic field of 130 G, which is close to optimal values for the Rb D2 transitions [51]. Circular polarization components (σ^+ and σ^-) generate Zeeman absorption profiles, frequency shifted symmetrically in opposite directions. After conversion (with a quarter-wave plate) and spatial separation (with PBS0), the orthogonal linearly polarized beam components are detected with photodiodes (PD1, PD2). Subtraction of both profiles by the low noise differential amplifier provides a broad dispersion signal (with monotonic slope) that is compared to the reference voltage. The locking point can be tuned continuously, either optically by rotating the quarter-wave plate, or electronically (with higher precision) by changing the reference voltage. The resulting error signal is fed to an external PID based servo. Then, the feedback voltage is applied to a PZT input of the laser controller which induces changes in the position of the grating. It enables the correction of frequency drifts and low-frequency noise. The detection part of the setup is enclosed in a housing to keep the photodiodes at the same temperature and protect them from ambient light. Except for advantages such as the simplicity of a dither-free scheme, wide capture range and the relatively broad ~400 MHz continuous range of stabilization around the Rb D2 line, the method suffers also from some flaws. Dependence of vapor pressure on temperature, quality of optical components, drifting electronics, and beam intensity noise contribute to the lock point instabilities, necessitating periodic adjustments. However, ability to stabilize the laser at an arbitrary detuning, robustness, and simplicity of configuration (with limited number of components) are the great merits of this method. The fluorescence signal monitored by the CCD camera is used for a coarse frequency control, while the fine frequency calibration is performed using the sub-Doppler reference spectrum, as discussed in section 2.4. Under typical conditions, without room temperature control and special efforts, a slow drift below 0.5 MHz/15 min (and below 2 MHz/h) is observed for the lock point set in vicinity of the ^{85}Rb $5S_{1/2}(F=3) \rightarrow 5P_{3/2}$ ($F'=2, 3, 4$) transitions.

2.3. Double-pass AOM frequency shifter

AOMs are used in applications where precise sweeping of the laser frequency or its on demand setting at a fixed detuning is required. Beside ability to control the beam frequency and intensity, AOM deflects the beam by an angle dependent on its driving radio frequency (RF). When frequency sweeps or jumps are foreseen, these undesired angular variations create serious problems with the alignment of downstream components (e.g., fibres). A useful solution is an AOM in a double-pass configuration which doubles the frequency offset, widens the tuning bandwidth and, at the same time, significantly reduces beam pointing fluctuations [83]. Also, higher multi-pass schemes, odd [84] or even [85], high diffraction orders [86] or combinations thereof [87] can be employed to expand the range of frequency shifts.

The Crystal Technology 3080–125 model (with centre frequency of 80 MHz and bandwidth of 25 MHz) with a dedicated 1080AF driver based on a voltage-controlled oscillator (VCO) has been used. The driver is supervised by a (laboratory-made) digitally controlled source providing: (i) a 0−15 V tuning voltage (calibrated in MHz for convenience) that allows for a fine RF tuning in absolute or relative increments, and (ii) a 0−1 V control voltage for RF power control. An optical setup includes two identical lenses L (of $f = 160$ mm, temporarily the uncoated ones are used), quarter- and half- wave plates, diaphragms, and the mirror M2. The half-wave plate matches the linear beam polarization with the axis of the AOM crystal. When properly aligned, the input beam is focused on the AOM aperture and, after being diffracted, passes through the lens and quarter-wave plate before being reflected into the modulator to undergo a second diffraction. The setting is optimized by maximizing the diffracted power. By careful disentangling the non-diffracted beams and spurious beam orders, the diffraction order −1 (or +1) is selected at each pass to accomplish optical frequency down-shift (or up-shift, respectively). The quarter-wave plate transforms the polarization so that the twice-diffracted beam can be separated from the input beam on the PBS2 splitter. Matching the beam waist and the AOM apertures is important for system efficiency [83].

The relative response of the AOM in the double-pass configuration as a function of the RF driving frequency in MHz is shown in Fig. 2(a) for the −1 order and in Fig. 3(a) for the +1 order. Substantial intensity variation and asymmetry with respect to the specified centre value is seen. The graphs look similar, but the optical frequencies are red-shifted [in Fig. 2(a)] or blue-shifted [in Fig. 3(a)] by twice the RF frequency applied. The measured peak diffraction efficiency in both configurations is of ~40% and

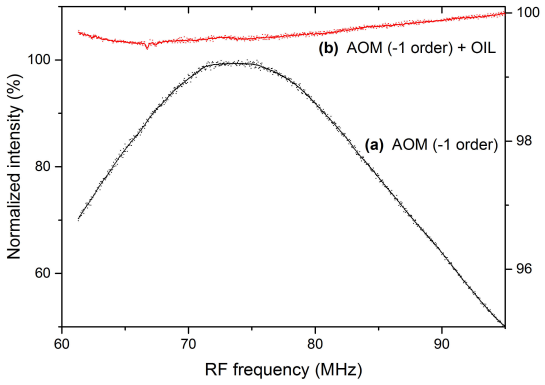

Fig. 2. Relative response of two systems as a function of the RF frequency (in MHz): (a) AOM only [lower trace (black curve), left vertical scale]; (b) AOM + OIL [upper trace (red curve), right vertical scale]. In (b), optical limiting of the OIL amplifier is revealed. Double-pass AOM is aligned in the –1 order, inducing an optical frequency down-shift.

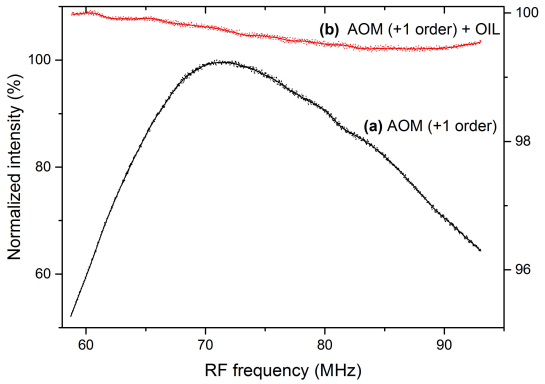

Fig. 3. Similar to Fig. 2, but here the double-pass AOM is aligned in the +1 order, inducing an optical frequency up-shift. Note different vertical scales for both curves.

its (optical) bandwidth is of 70 MHz. (Note: Fresnel reflections on two uncoated lenses in the AOM system contributed to the observed low diffraction efficiency.) The RF precision related mainly to the stability of the VCO is several tens of kHz. Thus, without compromising stability of the frequency lock, an offset centred around +160 MHz (or −160 MHz) and tuned in a bandwidth of ~70 MHz adds up to the master laser frequency. Although quite narrow, this bandwidth covers interesting features of the Rb spectrum and allows a precise detuning by several linewidths from the investigated resonance. The combined losses, however, reduce the available peak power to just ~2 mW.

2.4. *Optical injection-locking*

Optical injection of DLs has been actively researched and used in various applications [69, 70, 88, 89]. In the optical injection, a signal from a low-power single-frequency master laser is injected into a free running slave laser operating above threshold. Under various operating conditions, the slave may exhibit many dynamic states [70]. Two basic parameters that can be adjusted during an experiment and affect the behaviour of the injected laser are: the detuning $\Delta\nu = \nu_m - \nu_s$ between the frequencies of the master (ν_m) and the free running slave (ν_s) lasers, and the injection ratio $R = P_{inj}/P_0$, where P_{inj} and P_0 are the injected signal and the free-running slave powers, respectively. In the stable optical OIL regime, the slave laser replicates the frequency and linewidth of a weak seed beam and amplifies its power while maintaining phase locking between both beams. A stable OIL occurs for R above some minimal level (locking threshold) and for a range of detunings (most often negative) within certain boundaries $\Delta\nu^{lock}_{min} < \Delta\nu < \Delta\nu^{lock}_{max}$. A locking range defined as $\Delta\nu_{LR} = \Delta\nu^{lock}_{max} - \Delta\nu^{lock}_{min}$ is a useful parameter related to the OIL stability, its width (depending on P_{inj}) is proportional to the square root of R [88]. Thus, a higher R results in a broader $\Delta\nu_{LR}$ which makes it easier to lock the slave laser. In our setup, the slave laser (DL2 in Fig. 1) and its collimator are held in a collimation tube (Thorlabs LT230P-B) fixed in a solid aluminium block and mounted via TEC on the heat sink. The laser enclosed in its aluminium housing is current and temperature stabilized with controllers of the type described above. To initiate the OIL a few requirements should be addressed:

(i) *Mode matching, polarization matching, alignment.* To inject the seed beam into the slave aperture, both seed and slave beams need to have a similar spot size and shape. This condition is relaxed by the fact that DL2 and its collimator are of the same type as their counterparts in the master module. While the more accurate mode matching could result in a stronger coupling, no additional beam shaping was performed. The single stage optical isolator IS2 (Isowave I-7090-CH, 40 dB of ~85% transmission) protects the slave laser against back-reflections, as well as backward emission from the TA, and simultaneously allows injection through its escape port. The half-wave plate allows to maximize the isolator throughput and to match the polarization of the seed and slave beams. The overlapping of the beams is carried out by the adjusting mirrors (M3, M4) and the collimator. Due to the small size of the facet, careful monitoring of the light entering the laser waveguide is required. Authors have observed that the voltage build-up at a zero-bias laser junction is a useful criterion for injection optimization. Therefore, the current controller has a dedicated add-on function that measures the voltage directly at the junction when the bias current is off and the protective relay remains open. With the seed power of up to ~2 mW (measured upstream of the isolator escape port), the signal spans 0.7–2.2 V, providing a sensitive optimization method. In this approach, there is no need to open the case, disconnect or re-wire the DL before measurements. Alternatively, the voltage drops across a 10 kΩ resistor connected in parallel to the junction were measured over a convenient range of 0–1.4 V. However, the resistor should be connected carefully due to the risk of damaging the diode. Once the OIL is provisionally established, the master power is reduced, and the seed beam is re-aligned by maximizing injection efficiency. (While preparing the manuscript, authors found a similar approach, but with the DL disconnected from the controller which was used in Ref. 90).

(ii) *Injection strength and frequency matching.* The free-running laser DL2 biased far above the threshold at ~80–120 mA (~2–3I_{th}) emits up to ~50 mW, as measured behind the isolator. The injection power measured at the escape port of isolator IS2 has a range of ~0.8–2 mW for different AOM arrangements and RF frequencies,

however, the actual injection levels may have a higher dynamic range due to the residual beam pointing variation. No efforts were undertaken to determine the exact power coupled into the waveguide, but it has proven adequate for stable OIL in the applied operating conditions. (Even quite low injection powers may be sufficient for stable OIL operation [69, 70].) For the fixed operating conditions of the master laser, the slave frequency is being fine-tuned by temperature and current control until the frequencies ν_m and ν_s match closely. Typically, the OIL takes place in narrow (< 0.5 mA) current windows separated by ~10–15 mA intervals (similar quasi-periodic behaviour was investigated in Ref. 91), which facilitates optimization of both the output power and the locking range. The latter is done by changing the slave current (and temperature) while sweeping the master frequency and monitoring the OIL stability with a diagnostic system.

(iii) *Diagnostics.* Part of the beam split off with a variable beam divider (a half-wave plate and PBS3) is sent to the saturated absorption spectroscopy (SAS) system [6] in a simple single-beam configuration. It consists of a room temperature Rb vapor cell SC2 (Thorlabs GC19075-RB, 75 mm length), a partially reflecting (~10%) mirror Z1, quarter-wave plate, polarizing beam splitter PBS5, and a photodiode PD3. The beam frequency can be swept with the grating (displaced by the PZT actuator) or the AOM. The SAS signal allows a frequency calibration using the known sub-Doppler features as a reference [92, 93], helps extend the locking range and provides hints on frequency stability and spectral purity. Unstable or multi-mode operation is revealed as a shivering or noisy spectrum. The special role of SAS is to establish the origin for the AOM frequency sweeps, by offset tuning the master frequency relative to the selected spectral feature. As an auxiliary tool, a CCD camera enables continuous monitoring of the Rb fluorescence. A fraction of the beam is fed to the spectrum analyser FPI (Toptica FPI 100, FSR = 1 GHz, finesse > 500) to monitor the slave spectrum and OIL evolution. With the slave off, the seed beam that is partially reflecting off its front facet can also be analysed. Thus, the same system can be used to test both beams.

Once established, OIL is stable and reliable. The slave recreates the spectral properties of the weak signal beam and amplifies the power to its free-running generation level of up to ~50 mW. The OIL locking bandwidth covers the available MHF range (~2 GHz) of the ECDL used. In previous research with ECDL of ~5 GHz MHF tunability (based on the DL of another brand), after enabling the additional synchronization between the PZT tuning voltage and the slave current, a stable OIL over this wider bandwidth was observed. (Typical locking ranges amount of ~10 GHz [70]).

Figures 2(b) and 3(b) depict the normalized response of the OIL stage injected with the AOM detuned beam (double-pass AOM aligned in −1 or +1 order, respectively) as a function of the RF carrier frequency. Note: different vertical scales apply for curves (a) and (b). Two factors play a role: (i) input power dynamic range of at least ~1:2, (ii) variation of the RF frequency (optical frequency) in the range of ~35 MHz (~70 MHz, respectively). An almost flat response is observed. The output power is unaffected by changes in the signal intensity, an advantageous fact with practical implications [90, 94, 95]. The OIL stage thus acts as an all-optical limiting amplifier, effectively suppressing variations in the input signal strength (and intensity jitter). On the other hand, a frequency dependent effect can be seen. Power varies almost linearly with frequency, increasing [in Fig. 2(b)] or decreasing [in Fig. 3(b)] by at most ~0.5% in the available band. This behaviour is characteristic of a semiconductor OIL amplifier where in the locked regime the output increases linearly as the signal tunes red [69]. (Notes: (i) it is not clear why the monotonicity breaks down close to the low (high) RF limit in Fig. 2(b) [Fig. 3(b), respectively] which corresponds to the blue limit of the frequency band; (ii) stability of the injection-locked slave after injection with the AOM detuned seed was reported in Ref. 96).

The OIL stage replicates the spectral (frequency and linewidth) and spatial properties of the signal beam while offering high power. Acting as a strongly saturated all-optical limiting amplifier, it delivers a constant output power at a predefined limiting value (~50 mW) for optical signals of widely varying strength. As the optical frequency of the signal (within locking range) decreases, the OIL output power increases (nearly) monotonically. For our bandwidth of 70 MHz, the effect amounts ~0.5 %. Another advantage is the correction of residual pointing fluctuations of the seed beam that occur during frequency tuning with the AOM or PZT. This enables the OIL amplified beam to be stably and efficiently coupled to the small apertures of the next amplifier or optical fibre.

The OIL properties, when applied to sub-Doppler spectra registration, are illustrated in Fig. 4 and Fig. 5. The figures show two saturated absorption features of the ^{85}Rb D2 line (recorded with the arrangement in Fig. 1) crossover resonances: F = 3 → F' = (2,4) (left peak) and F = 3 → F' = (3,4) (right peak), 31.5 MHz apart. Detuning is accomplished with a double-pass AOM and measured relative to the origin defined by the DAVLL locked frequency of the master laser. The AOM is aligned in the −1 (in Fig. 4) or +1 (in Fig. 5) order, hence the horizontal scales and their origins differ. The spectra in Fig. 4(a) and Fig. 5(a) are recorded with the beam directly after the AOM. Serious distortions are seen, line shapes are deformed, and their centres shifted. In contrary, spectra in Fig. 4(b) and Fig. 5(b) are recorded with the beam after passing AOM and the OIL amplifier. The OIL stage compensates for changes in the AOM signal level so that undistorted spectra are observed. Note that in the spectra, the Doppler broadened pedestal is not subtracted, and the linewidths are power broadened. The subtle modulation structure visible in Fig. 5(b) results from mechanical disturbances during the measurement time (~0.5 s). The spectra demonstrate the suitability of our system for precise measurements.

2.5. *Power booster*

Higher power is achieved by injecting the OIL amplified beam into the TA. Contrary to the OIL where the seed beam frequency and working parameters of the amplifier are strongly interrelated, the TA is not critically sensitive to the bias current and temperature and can amplify frequencies across its broad gain profile. In our system the m2k-laser GmbH TA-0780-1000-CM device was used; with 780 nm centre wavelength, 767–787 nm

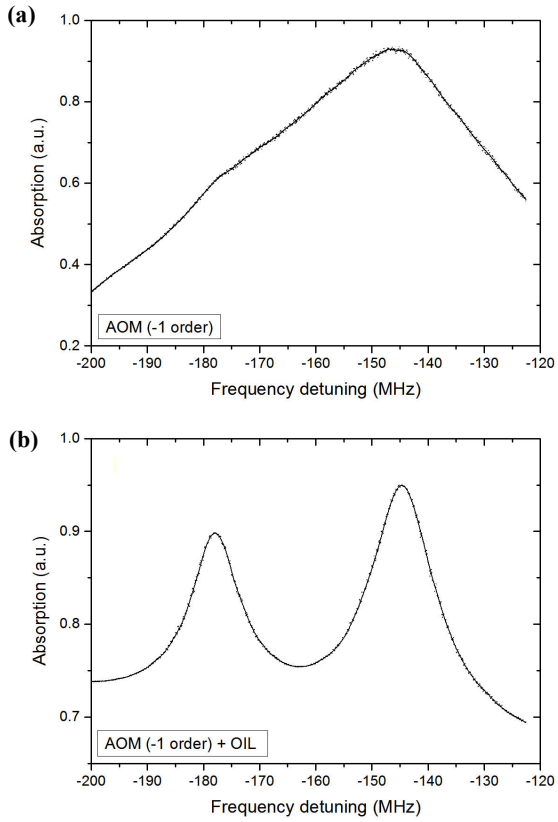

Fig. 4. Saturated-absorption sub-Doppler features of the ^{85}Rb D2 transition recorded by scanning laser frequency with the double-pass AOM aligned in the −1 order. The crossover resonances F = 3 → F' = (2,4) (left peak) and F = 3 → F' = (3,4) (right peak) separated by 31.5 MHz are shown. Laser beam is taken: (a) directly after the AOM. Distortions are caused by a strong dependence of the AOM diffraction efficiency on RF frequency; (b) after passing AOM and the OIL amplifier. The spectrum recovers its regular shape due to optical limiting capability of the OIL amplifier. Note: the lines are power-broadened, and the Doppler pedestal is not subtracted.

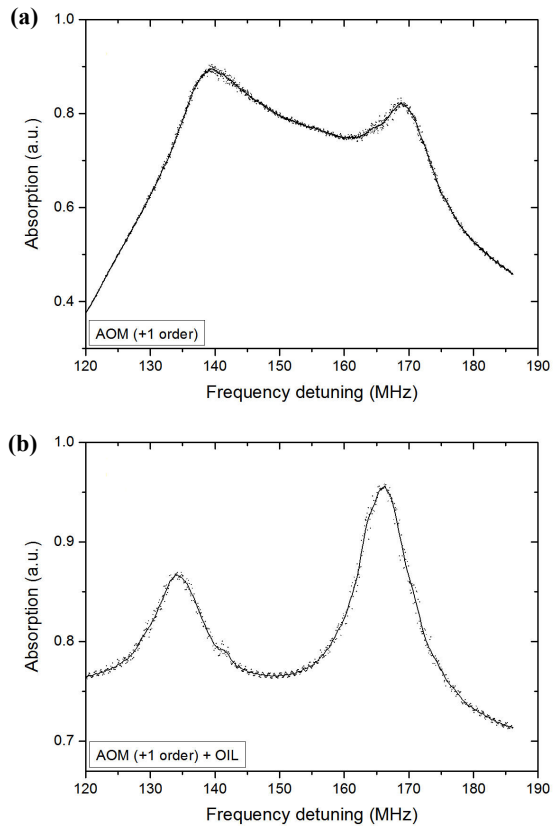

Fig. 5. Similar to Fig. 4, but here the double-pass AOM is aligned in the +1 order.

gain bandwidth, 1 W specified output power, 2 mm length, 20–30 mW suggested seed power, 2.1 A operation current, TM polarization (i.e., parallel to the fast axis), and $M^2 = 1.3$ beam quality factor. A bare, and thus vulnerable, semiconductor structure fixed onto the C-mount consists of two sections: a short and narrow pre-amplifying ridge-waveguide acting also as a mode filter, and a long power amplifying tapered section. The width of the exit (entrance) aperture is of 205 µm (~3 µm, respectively). Both facets are quality (<0.01%) AR-coated. Two copies of the amplifier were ordered, and one extra was kindly offered for testing purposes, with possibly inferior spatial properties of the beam. Originally, it was planned to be used only during the system assembly and first tests when the risk of failure seemed to be particularly high. The TA handling should be careful to avoid static discharge, laser light induced break-down, mechanical damage, or contamination. However, as the diode performed better than expected, authors extended its use. The results below are for this TA chip.

Various designs of TA modules have been proposed, e.g., [68, 73–77, 97]. Our design is inspired by Ref. 75. The C-mount package (containing the TA chip) is bolted into the slot in the precision-machined copper block, thus securing a good electrical and thermal contact. The block is fixed firmly with screws inside a rectangular (40×60×60 mm^3) aluminium enclosure with two holes of 20 mm diameter centred along the optical axis. Inside the enclosure, there is a small PCB containing wiring for power and control, a Schottky diode (BAT 85) to protect against a reverse voltage above 0.3 V and a miniature relay (Axicom IM03) (with another Schottky diode as a shunt) which shortens the TA when the current is off. To reduce strain on the TA structure, its cathode connection (a delicate wire flag attached to the ribbon) is soldered with a short lead to the protective board. Another wire connects the anode (C-mount) and the copper block to the PCB. To improve the heat transfer and avoid the use of thermal compound, an indium foil is applied between the C-mount and the copper block and on other relevant surfaces. The temperature (at the recommended value of 20 ºC) is stabilized by the LM35 sensor embedded near TA, the TEC sandwiched between the back of the enclosure and the aluminium base, and the controller of the same type as mentioned earlier. The massive base is attached to the optical board for stability and heat dissipation. Because of moderate power no water cooling is used. To run the device, a 2.5 A current controller is designed, some functions of which are similar to the previously described high-precision power supply.

To simplify the system, readily available components have been used. The seed beam is focused on the TA entrance facet by a lens of the same type as used in the OIL and master lasers. The output is shaped using an aspheric lens (Thorlabs C330TME-B, $f = 3.1$ mm, $NA = 0.68$, AR-coated) and an additional cylindrical lens to compensate for astigmatism. Both aspheric lenses are held in the threaded

adapters (Thorlabs S05TM09) and adjustable lens tubes (Thorlabs SM05V05), and then mounted in the biaxial positioning lens holders (Thorlabs SCP05), thus providing axial and transverse adjustment of both collimators. The lens holders, in turn, are fixed in the mirror mounts (Thorlabs KS1), which are attached to both ends of a solid aluminium plate ($150\times40\times15$ mm^3). The plate is rigidly fixed to the floor of the TA enclosure. Conically shaped nitrile rubber gaskets fitted between the lens tubes and the openings in the enclosure, provide tight yet elastic seals to protect against dust and humidity ingress. The fully assembled TA head is shown in Fig. 6. Its ultimate performance depends on a careful alignment. Fine threaded adjusters enable a precise positioning of the collimators in all axes. The TA power supply was not equipped with the previously described functionality for optimizing the injection efficiency. Guidance on the TA alignment procedure can be found, e.g., in Ref. 77. In brief, the incoming beam is set to be collinear with the amplified spontaneous emission (ASE) emitted from the rear facet of the unseeded TA. For an ideal coupling efficiency, the waist of the collimated seed beam should lie in the entrance facet of the TA waveguide, while its diameter and the divergence angle should coincide with the values for the backward emitted beam [97].

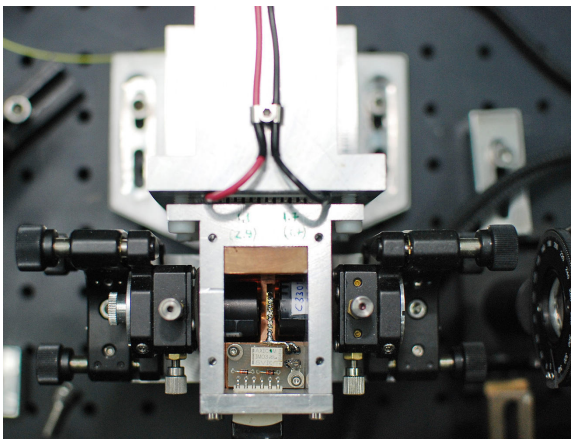

Fig. 6. Fully assembled TA head with the lid open. The TA chip (not visible) fixed to the copper block is situated between the input and output collimator tubes. The latter are mounted in their respective xy translation stages and kinematic mirror mounts to enable alignment. A small PCB contains wiring, protection diodes, relay, and miniature connector. TA enclosure is attached to the aluminium heat sink, and TEC is sandwiched in between. The beam propagates from left to right.

The TA output beam is characterized by (i) various divergences in directions parallel (slow axis) and perpendicular (fast axis) to the waveguide plane, with angles (including 95% power) of 17° and 45°, respectively, and (ii) strong astigmatism in the slow axis. While the beam waist in the fast axis is at the exit facet, the (virtual) beam waist in the slow axis is located in the plane of the waveguide at a depth of about L/n_g behind the facet, where L is the length of the tapered section and n_g is the effective refractive index [61]. Assuming $L = 1.5$ mm, $n_g = 3$, the depth is of ~0.5 mm and depends on the bias current. Therefore, in addition to an aspheric lens ensuring collimation in the fast axis, a cylindrical AR-coated lens is used to correct the astigmatism in the slow axis. Its focal length $f = 75$ mm was selected taking into account the spatial constraints of the system. A double-stage optical isolator IS3 (Gsänger DLI-1, >60 dB, aperture of 5 mm, transmission of ~85%) placed behind the cylindrical lens prevents feedback into the TA. The collimated beam is horizontally elongated (diameter ~3 mm) with the aspect ratio of ~5:3. Further beam shaping can be done with an anamorphic prism pair (to improve circularization) and/or telescope (to change diameter). It is known that the spatial mode quality of the TA output is not as good as that of the narrow waveguide device. While in the fast axis the intensity distribution follows the Gaussian profile, in the slow axis, the pattern is less regular, therefore a pinhole or coupling into fibre can be used for spatial mode cleaning.

The power characteristics of the TA are shown in Fig. 7. The input (output) power is measured before the collimator (after the isolator, respectively). The seed power is varied by a half-wave plate mounted in the motorized rotation stage (Thorlabs PRM1Z8), slightly tilted to prevent feedback, followed by a polarizing beam splitter PBS4 placed just behind it. Figure 7(a) shows the dependence of the TA output on the seed power (from 0.4 mW to 40 mW) for currents from 0.8 A to 2.2 A. (Note: currents above 1.5 A are not recommended in the unseeded TA.) For each current, the output power increases with the

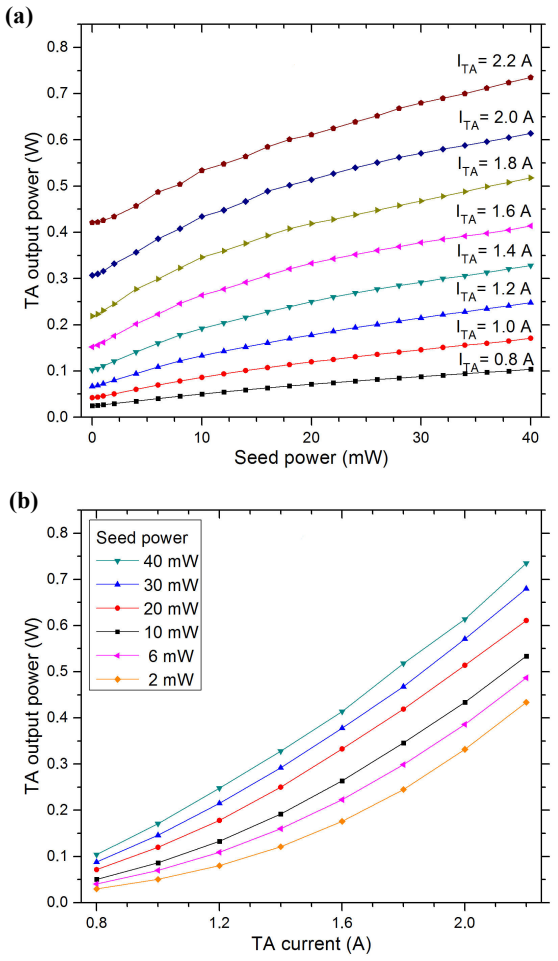

Fig. 7. Power characteristics of the TA stage. (a) Output power as a function of the input (seed) power for different operating currents. The lowest (highest) input power is 0.4 mW (40 mW). (b) Output power as a function of the operating current for selected values of the seed power.

seed power, but the growth rate gradually slows down, indicating partial saturation. For smaller currents, saturation is more pronounced and starts at lower input powers. Figure 7(b) shows the output power as a function of the current for selected seed powers. There is a pronounced increase in power when the current exceeds the threshold value of ~0.6–0.8 A. For example, at a seed of 12 mW (20 mW) and a current in the range of 1.6–2.2 A, an almost linear growth is observed with a slope coefficient of 0.45 W/A (0.46 W/A, respectively). As the seed power increases, the slope increases and the threshold current decreases. In Ref. 77, for the TA of the same type and under similar conditions (seed power of 12.6 mW and the output power measured after the isolator) a 0.41 W/A slope is reported. In typical working conditions with a current of 1.9 A and a seed power of 12 mW (20 mW) an output of 404 mW (467 mW) was observed, which translates into an amplification factor of 33.7 (23.3) or a gain of 15.3 dB (13.7 dB, respectively). In Ref. 77, for a current of 1.9 A similar to a 430 mW output power and a 15.3 dB gain (or 565 mW and 16.5 dB gain, when measured before the isolator) is reported, which compares favourably with the manufacturer data. Thus, our power data seem to agree well with those in Ref. 77 for the same TA chip. However, the output power is slightly below expected levels. The above may suggest that the TA characteristics have not reached optimum. Optical losses are the obvious reason (15% in the isolator alone). The efficiency of injection also depends on the seed beam polarization, which should coincide (within a few degrees) with the direction specified for the TA. However, its control is ensured with the half-wave plate placed in front of a TA input. Inefficient coupling can impair the TA efficiency. Several factors affect power injected into the waveguide: inaccurate collimation and focusing (the waist diameter), inadequate matching of the waist with the TA input facet (shift between the axes of the beam and TA, or angular tilt) [97]. It was concluded that the coupling of the seed power to the waveguide may not have been fully optimized.

The TA maintains a spectral quality of the input beam [73]. Our analysis with the spectrum analyser and the SAS spectrometer showed no signs of broadening of the linewidth as compared to the master beam. However, the output beam, in addition to a narrow, coherent peak, consists of a broadband pedestal due to the amplified spontaneous emission (ASE). The ASE power and its fraction in the total output varies with the TA operating conditions. It is highest at low seed levels and high injection currents. For the unseeded TA, the ASE of 5.6 mW (35.8 mW) at 0.5 A (1.5 A, respectively) was observed. No attempt was made to estimate the exact contribution of ASE to the results in Fig. 7, however, especially for low seed powers and medium to high operating currents, this share is significant. Under working conditions, the gain is depleted by the signal being amplified and thus, the ASE is attenuated. As shown in Refs. 68 and 76, the ASE fraction decreases sharply with increasing seed power, as the gain saturates. At full saturation, fractions up to a few percent (the value depending on the temperature) [68] (~10% [76]) are reported for various 780 nm devices. Since the power spectral density in a narrow, coherent peak is several orders of magnitude greater than in the ASE pedestal, in some important applications (e.g., in laser cooling), the impact of the ASE is negligible [68, 77].

Optical fibre, single-mode (SM) or polarization maintaining (PM), is an effective way to guide a laser beam while improving its spectral and spatial quality. The prerequisite for coupling the TA light into the fibre is optimization of alignment and collimation of the beam. Since the beam is astigmatic, with different waist positions, focal lengths, and divergences in the fast and slow axes, a separate collimation in both directions is required. The following procedure was used. After initial alignment of the aspheric and cylindrical lenses, at very low output power, the spot size and beam height were checked (with calibrated ruler, irises, IR viewer and/or CCD camera) at different distances, up to several meters, from the source. After multiple iterative adjustments of lenses, a beam was formed (set parallel to the bench top, at the required height) with a very little divergence along the entire distance. This was considered evidence of adequate collimation. The procedure was then repeated for the TA under intermediate operating conditions, but with the intensity reduced to a safe level by means of a variable beam splitter (half-wave plate and PBS, not shown in Fig. 1) positioned directly after the IS3 isolator. (Note: another way to reduce the intensity is to use several coated or uncoated wedges.) After achieving the appropriate collimation, the fibre coupler (Thorlabs PAF-X-15-B, $f = 15.4$ mm, $NA = 0.16$, clear aperture of 5 mm, AR range of 600–1050 nm) was inserted into the apparatus. To facilitate the proper alignment, in front of it there were two irises (set at the required height and at a distance from each other; not shown in Fig. 1) and two beam steering mirrors (M10, M11). After many iterative adjustments to their settings, the beam passed exactly through the centres of the irises and the centre of the coupling lens aperture.

Good fibre coupling requires precise positioning of the fibre core relative to the focused beam (with the waist centred on the core, and the waist size and beam divergence comparable to the diameter of the core and NA of the fibre). For a multimode (MM) fibre with a wide core (typically tens of μm or more), the coupling is easier than in the case of an SM (or PM) fibre with a narrow (several μm) core. Therefore, the MM fibre was first attached to the coupler to facilitate its initial setup. The coupling was optimized by adjusting screws in the coupler, while monitoring the transmitted signal. After maximizing the throughput, the MM fibre was removed and the PM patch cable (Thorlabs P5-780PM-FC-5, $NA = 0.12$, core diameter of ~5 μm) was attached. To prevent back reflections, the fibre with a tilted facet on the input side was used (FC/APC connector). The half-wave plate adjusted the beam polarization to the appropriate axis of the fibre. Coupler adjustment steps were iterated in accordance with the manufacturer's guidelines. In parallel, efforts were made to: (i) optimize the position of the cylindrical (and aspheric) lens, and (ii) tweak the seed alignment. (Note: the auxiliary laser beam propagating backwards along the fibre can facilitate the positioning of elements by overlapping the TA beam at two different points.)

The coupling efficiency was preliminary tested for several intermediate and high TA currents and seed powers. Our very provisional results are as follows. For a seed of 25 mW, a current of 1.6 A, and an output power of

360 mW, authors achieved the value of ~25%, however, for higher bias currents, the efficiency tended to gradually decline (the latter may be related to a decrease in the spatial quality of the beam). There may be several reasons for this modest result, as, e.g., inadequate beam shaping (the TA beam was not circular, hence the incident field distribution differed from the fibre mode) or inaccurate (despite efforts) TA alignment. Other authors reported for TA beams the coupling efficiency of the SM fibre: 25–35% [77], 46% [68], 45–55% [75], or > 50% [97]. For the PM fibre, a high efficiency of 70% was reported in Ref. 74.

Better collimation and alignment on the input side might improve the seed beam mode matching and thus increase the TA power efficiency. For a better fibre coupling, an improved circularization and astigmatism compensation are considered [97]. In its present form, the TA stage requires small adjustments before reaching thermal equilibrium, each time the beam is to be used, or occasionally, to compensate for long term drifts. The entire system is mounted on an optical board of 0.6×1.2 m^2, offering limited portability.

3. Conclusions

A three-stage amplifying frequency-stabilized DL based system was presented, designed for precise measurements where a high-quality, high-power beam is required. The system operating at 780 nm produces a nearly diffraction-limited beam of a 0.6 MHz linewidth and a power above 700 mW, tunable in vicinity of the D2 lines of both isotopes of Rb atoms. Various components of the system, in particular lasers and high precision controllers, have been fully designed and manufactured in our laboratory.

Properties of the OIL stage have been analysed. OIL replicates the spectral and spatial properties of the signal beam, while amplifying its power. The OIL stage acts as a strongly saturated all-optical limiting amplifier that stabilizes the output power at a predefined value for widely differing input signal strengths. The same mechanism also suppresses amplitude fluctuations of the signal. Optical limitation based on various mechanisms is of interest in many fields [90, 94, 95, 98]. However, authors are not aware of any reports on the application of this property directly to the registration of spectra in an OIL based system using the AOM frequency sweep. Therefore, authors found it useful to demonstrate the limiting capability of the system with high resolution sample spectra. Another advantage of the OIL stage is compensation of slight pointing fluctuations of the seed beam when its frequency is swept by the AOM (or PZT). There is no sign of beam shift or deflection after the OIL stage. It enables the OIL amplified beam to be stably coupled to the small facets of the next stage amplifier or fibre.

An approach was developed to optimize injection efficiency, where the light-induced increase in voltage at the junction, operated in a photovoltaic mode, is directly measured by the laser controller, without the need to disconnect or re-wire the DL.

Our arrangement employs simple uncoated FP DLs, while TA chips are common and available for many wavelengths. The system requires relatively few optical components. As compared to the BAL based systems, the arrangement of the TA ones is simpler, the spectral and spatial beam quality is better, and usually less seed power is needed [61]. Thus, a simple reliable and relatively easy-to-operate tunable laser system of significant power has been developed.

The central part of our system is the tunable single-frequency ECDL (master) which includes several optical and mechanical elements that require fine adjustment. Alternatively, the distributed feedback (DFB) DL can be used, which, due to its advanced design, offers many advantages along with the simplicity of a compact package without moving parts. In the DFB DL, a Bragg grating is integrated into the laser waveguide and set parallel to the direction of beam propagation, that results in several unique properties. The important advantages of the DFB lasers include a very good monochromaticity: the single longitudinal mode of a narrow linewidth (~1–10 MHz in a free-running laser) allows for many applications, lasers have also a high side mode rejection ratio (up to 40–50 dB), that enables high frequency modulation. DFB DLs are frequency stabilized and tuned continuously (in the range of several nm, MHF range > 1 THz) by the temperature (~−25 MHz/mK) and the current (~−1 MHz/μK) control [99]. DFB lasers outperform FP ones in many respects and are available in the near- and mid-IR with powers ranging from a few to a hundred mW.

During the preparation of the manuscript, authors learned of a related work [100] which presents the design and characteristics of the ECDL-TA 850 nm system and discusses the influence of thermal disturbances on its stability.

Authors' statement

Research concept and design, K. K., J. S., and M. G.; collection and/or assembly of data, K. K., J. S., and M. G.; data analysis and interpretation, K. K. and J. S.; writing the article, K. K. and J. S.; critical revision of the article, K. K., J. S., and M. G.; final approval of article, J. S. and M. G.

References

[1] Welch, D. F. A brief history of high-power semiconductor lasers. *IEEE J. Sel. Top. Quantum Electron.* **6**, 1470–1477 (2000). https://doi.org/10.1109/2944.902203

[2] Wieman, C. E & Hollberg, L. Using diode lasers for atomic physics. *Rev. Sci. Instrum.* **62**, 1–20 (1991). https://doi.org/10.1063/1.1142305

[3] Galbács, G. A review of applications and experimental improvements related to diode laser atomic spectroscopy. *Appl. Spectrosc. Rev.* **41**, 259–303 (2006) . https://doi.org/10.1080/05704920600620378

[4] Mroziewicz, B. External cavity wavelength tunable semiconductor lasers: a review. *Opto-Electron. Rev*. **16**, 347–366 (2008). https://doi.org/10.2478/s11772-008-0045-9

[5] Nasim, H. & Jamil, Y. Recent advancements in spectroscopy using tunable diode lasers. *Laser Phys. Lett.* **10**, 043001 (2013). https://doi.org/10.1088/1612-2011/10/4/043001

[6] MacAdam, K. B., Steinbach A. & Wieman, C. A narrow-band tunable diode laser system with grating feedback and a saturated absorption spectrometer for Cs and Rb. *Am. J. Phys.* **60**, 1098–1111 (1992). https://doi.org/10.1119/1.16955

[7] Merimaa, M. *et al*. Compact external-cavity diode laser with a novel transmission geometry. *Opt. Commun.* **174**, 175–180, (2000). https://doi.org/10.1016/S0030-4018(99)00654-9

[8] Laurila, T., Joutsenoja, T., Hernberg, R. & Kuittinen, M. Tunable external-cavity diode laser at 650 nm based on a transmission diffraction grating. *Appl. Opt.* **41**, 5632–5637 (2002). https://doi.org/10.1364/AO.41.005632

[9] Hoppe, M. *et al*. Construction and characterization of external cavity diode lasers based on a microelectromechanical system device. *IEEE J. Sel. Top. Quantum Electron*. **25**, 2700109 (2019). https://doi.org/10.1109/JSTQE.2019.2912059

[10] Hieta, T., Vainio, M., Moser, C. & Ikonen, E. External-cavity lasers based on a volume holographic grating at normal incidence for spectroscopy in the visible range. *Opt. Commun.* **282**, 3119–3123 (2009). https://doi.org/10.1016/j.optcom.2009.04.047

[11] Luvsandamdin, E. *et al*. Micro-integrated extended cavity diode lasers for precision potassium spectroscopy in space. *Opt. Express*. **22**, 7790–7798 (2014). https://doi.org/10.1364/OE.22.007790

[12] Rauch, S. & Sacher, J. Compact Bragg grating stabilized ridge waveguide laser module with a power of 380 mW at 780 nm. *IEEE Photon. Technol. Lett.* **27**, 1737–1740 (2015). https://doi.org/10.1109/LPT.2015.2438545

[13] Allard, F., Maksimovic, I., Abgrall, M. & Laurent, Ph. Automatic system to control the operation of an extended cavity diode laser. *Rev. Sci. Instrum.* **75**, 54–58 (2004). https://doi.org/10.1063/1.1634359

[14] Gilowski, M. *et al*. Narrow bandwidth interference filter-stabilized diode laser systems for the manipulation of neutral atoms. *Opt. Commun.* **280**, 443–447 (2007). https://doi.org/10.1016/j.optcom.2007.08.043

[15] Thompson, D. J. & Scholten, R. E. Narrow linewidth tunable external cavity diode laser using wide bandwidth filter. *Rev. Sci. Instrum* **83**, 023107 (2012). https://doi.org/10.1063/1.3687441

[16] Yang, W., Joshi, A., Wang, H. & Xiao, M. Simple method for frequency locking of an extended-cavity diode laser. *Appl. Opt.* **43**, 5547–5551 (2004). https://doi.org/10.1364/AO.43.005547

[17] Li, H. & Telle, H. R. Efficient frequency noise reduction of GaA1As semiconductor lasers by optical feedback from an external high-finesse resonator. *IEEE J. Quantum Electron*. **25**, 257–264 (1989). https://doi.org/10.1109/3.18538

[18] Hayasaka, K. Frequency stabilization of an extended-cavity violet diode laser by resonant optical feedback. *Opt. Commun.* **206**, 401–409 (2002). https://doi.org/10.1016/S0030-4018(02)01446-3

[19] Vassiliev, V. V. *et al*. Narrow-line-width diode laser with a high-*Q* microsphere resonator. *Opt. Comm.* **158**, 305–312 (1998). https://doi.org/10.1016/S0030-4018(98)00578-1

[20] Liang, W. *et al*. Whispering-gallery-mode-resonator-based ultranarrow linewidth external-cavity semiconductor laser. *Opt. Lett.* **35**, 2822–2824 (2010). https://doi.org/10.1364/OL.35.002822

[21] Ricci, L. *et al*. A compact grating-stabilized diode laser system for atomic physics. *Opt. Commun.* **117**, 541–549 (1995). https://doi.org/10.1016/0030-4018(95)00146-Y

[22] Arnold, A. S., Wilson, J. S. & Boshier, M. G. A simple extended-cavity diode laser. *Rev. Sci. Instrum.* **69**, 1236–1239 (1998). https://doi.org/10.1063/1.1148756

[23] Harvey, K. C. & Myatt, C. J. External-cavity diode laser using a grazing-incidence diffraction grating. *Opt. Lett.* **16**, 910–912 (1991). https://doi.org/10.1364/OL.16.000910

[24] Stry, S. *et al*. Widely tunable diffraction limited 1000 mW external cavity diode laser in Littman/Metcalf configuration for cavity ring-down spectroscopy. *Appl. Phys. B* **85**, 365–374 (2006). https://doi.org/10.1007/s00340-006-2348-1

[25] Nilse, L., Davies, H. J. & Adams, C. S. Synchronous tuning of extended cavity diode lasers: the case for an optimum pivot point. *Appl. Opt.* **38**, 548–553 (1999). https://doi.org/10.1364/AO.38.000548

[26] Saliba, S. D., Junker, M., Turner, L. D. & Scholten, R. E. Mode stability of external cavity diode lasers. *Appl. Opt.* **48**, 6692–6700 (2009). https://doi.org/10.1364/AO.48.006692

[27] Petridis, C., Lindsay, I. D., Stothard, D. J. M. & Ebrahimzadeh, M. Mode-hop-free tuning over 80 GHz of an extended cavity diode laser without antireflection coating. *Rev. Sci. Instrum.* **72**, 3811–3815 (2001). https://doi.org/10.1063/1.1405783

[28] Hult, J., Burns, I. S. & Kaminski, C. F., Wide-bandwidth mode-hop-free tuning of extended-cavity GaN diode lasers. *Appl. Opt.* **44**, 3675–3685 (2005). https://doi.org/10.1364/AO.44.003675

[29] Vassiliev, V. V., Zibrov, S. A. & Velichansky, V. L. Compact extended-cavity diode laser for atomic spectroscopy and metrology. *Rev. Sci. Instrum.* **77**, 013102 (2006). https://doi.org/10.1063/1.2162448

[30] Führer, T., Stang, D. & Walther, T. Actively controlled tuning of an external cavity diode laser by polarization spectroscopy. *Opt. Express* **17**, 4991–4996 (2009). https://doi.org/10.1364/OE.17.004991

[31] Repasky, K. S., Nehrir, A. R., Hawthorne, J. T., Switzer, G. W. & Carlsten, J. L. Extending the continuous tuning range of an external-cavity diode laser. *Appl. Opt.* **45**, 9013-9020 (2006). https://doi.org/10.1364/AO.45.009013

[32] Boshier, M. G., Berkeland, D., Hinds, E. A. & Sandoghdar, V. External-cavity frequency-stabilization of visible and infrared semiconductor lasers for high resolution spectroscopy. *Opt. Comun.* **85**, 335–359 (1991). https://doi.org/10.1016/0030-4018(91)90490-5

[33] Dutta, S., Elliott, D. S. & Chen, Y. P. Mode-hop-free tuning over 135 GHz of external cavity diode lasers without antireflection coating. *Appl. Phys. B* **106**, 629–633 (2012). https://doi.org/10.1007/s00340-011-4841-4

[34] Zhu, Y., Liu Z., Zhang, X., Shao, S. & Yan, H. Dynamic mode matching of internal and external cavities for enhancing the mode-hop-free synchronous tuning characteristics of an external-cavity diode laser. *Appl. Phys. B* **125**, 217 (2019). https://doi.org/10.1007/s00340-019-7335-4

[35] Lotem, H., Pan, Z. & Dagenais, M. Tunable external cavity diode laser that incorporates a polarization half-wave plate. *Appl. Opt*. **31**, 7530–7532 (1992). https://doi.org/10.1364/AO.31.007530

[36] Saliba, S. D. & Scholten, R. E., Linewidths below 100 kHz with external cavity diode lasers. *Appl. Opt*. **48**, 6961–6966, (2009). https://doi.org/10.1364/AO.48.006961

[37] Genty, G., Gröhn, A., Talvitie, H., Kaivola, M. & Ludvigsen, H. Analysis of the linewidth of a grating-feedback GaAlAs laser. *IEEE J. Quantum Electron.* **36**, 1193–1198 (2000). https://doi.org/10.1109/3.880660

[38] Loh, H. *et al*. Influence of grating parameters on the linewidths of external-cavity diode lasers. *Appl. Opt.* **45**, 9191–9197 (2006). https://doi.org/10.1364/AO.45.009191

[39] Talvitie, H., Pietiläinen, A., Ludvigsen, H. & Ikonen, E. Passive frequency and intensity stabilization of extended-cavity diode lasers. *Rev. Sci. Instrum.* **68**, 1–7 (1997). https://doi.org/10.1063/1.1147810

[40] Turner, L. D., Weber, K. P., Hawthorn, C. J. & Scholten, R. E. Frequency noise characterisation of narrow linewidth diode lasers. *Opt. Comm.* **201**, 391–397 (2002). https://doi.org/10.1016/S0030-4018(01)01689-3

[41] Bennetts, S. *et al*. External cavity diode lasers with 5 kHz linewidths and 200 nm tuning range at 1.55 μm. *Opt. Expr.* **22**, 10642–10654 (2014). https://doi.org/10.1364/OE.22.010642

[42] Sahagun, D., Bolpasi, V. & von Klitzing, W. A simple and highly reliable laser system with microwave generated repumping light for cold atom experiments. *Opt.Commun*. **290**, 110–114 (2013). https://doi.org/10.1016/j.optcom.2012.10.013

[43] Cook, E. C., Martin, P. J., Brown-Heft, T. L., Garman, J. C. & Steck, D. A. High-passive-stability diode-laser design for use in atomic-physics experiments. *Rev. Sci. Instrum.* **83**, 043101 (2012). https://doi.org/10.1063/1.3698003

[44] Libbrecht, K. G. & Hall, J. A low-noise high-speed diode laser current controller. *Rev. Sci. Instrum.* **64**, 2133–2135 (1993). https://doi.org/10.1063/1.1143949

[45] Lazar, J., Jedlička, P., Čip, O. & Ružička, B. Laser diode current controller with a high level of protection against electromagnetic interference. *Rev. Sci. Instrum.* **74,** 3816–3819 (2003). https://doi.org/10.1063/1.1593783

[46] Erickson, C. J., Zijll, M. V., Doermann, G. & Durfee, D. S. An ultra-high stability, low-noise laser current driver with digital control. *Rev. Sci. Instrum.* **79**, 073107 (2008). https://doi.org/10.1063/1.2953597

[47] Taubman, M. S. Low-noise high-performance current controllers for quantum cascade lasers. *Rev. Sci. Instrum.* **82**, 064704 (2011). https://doi.org/10.1063/1.3600602

[48] Meyrath, T. P. An analog current controller design for laser diodes. *Atom Optics Laboratory Center for Nonlinear Dynamics University of Texas at Austin*, https://atomoptics-nas.uoregon.edu/ta_circuit/meyrath_laser_diode.pdf (2003), (Accessed: 30th July 2021).

[49] Madhavan Unni, P. K., Gunasekaran, M. K. & Kumar, A. ±30 μK temperature controller from 25 to 103 °C: Study and analysis. *Rev. Sci. Instrum.* **74**, 231 (2003). https://doi.org/10.1063/1.1529299

[50] Libbrecht, K. G. & Libbrecht, A. W. A versatile thermoelectric temperature controller with 10 mK reproducibility and 100 mK

absolute accuracy. *Rev. Sci. Instrum.* **80**, 126107 (2009). https://doi.org/10.1063/1.3274204

[51] Millett-Sikking, A., Hughes, I. G., Tierney, P. & Cornish, S. L. DAVLL lineshapes in atomic rubidium. *J. Phys. B* **40,** 187–198 (2007). https://doi.org/10.1088/0953-4075/40/1/017

[52] Krzemień, L. *et al*. Laser frequency stabilization by magnetically assisted rotation spectroscopy. *Opt. Commun.* **284**, 1247–1253 (2011). https://doi.org/10.1016/j.optcom.2010.11.024

[53] Black, E. D. An introduction to Pound–Drever–Hall laser frequency stabilization. *Am. J. Phys.* **69**, 79–87 (2001). https://doi.org/10.1119/1.1286663

[54] Appel, J., MacRae, A. & Lvovsky, A. I. A versatile digital GHz phase lock for external cavity diode lasers. *Meas. Sci. Technol.* **20**, 055302 (2009). https://doi.org/10.1088/0957-0233/20/5/055302

[55] Chéron, B., Gilles, H. Hamel, J., Moreau, O. & Sorel, H. Laser frequency stabilization using Zeeman effect. *J. Physique III France* **4**, 401–406 (1994). (in French) https://doi.org/10.1051/jp3:1994136

[56] Corwin, K. L., Lu, Z.-T., Hand, C. F., Epstein, R. J. & Wieman, C. E. Frequency-stabilized diode laser with the Zeeman shift in an atomic vapor. *Appl. Opt.* **37**, 3295–3298 (1998). https://doi.org/10.1364/AO.37.003295

[57] Pustelny, S., Schultze, V., Scholtes, T. & Budker, D. Dichroic atomic vapor laser lock with multi-gigahertz stabilization range. *Rev. Sci. Instrum.* **87**, 063107 (2016). https://doi.org/10.1063/1.4952962

[58] Wąsik, G., Gawlik, W., Zachorowski, J. & Zawadzki, W. Laser frequency stabilization by Doppler-free magnetic dichroism. *Appl. Phys. B* **75**, 613–619 (2002). https://doi.org/10.1007/s00340-002-1041-2

[59] Harris, M. L., Cornish, S. L., Tripathi, A. & Hughes, I. G. Optimization of sub-Doppler DAVLL on the rubidium D2 line. *J. Phys. B: At. Mol. Opt. Phys.* **41**, 085401 (2008). https://doi.org/10.1088/0953-4075/41/8/085401

[60] Marchant, A. L. *et al*. Off-resonance laser frequency stabilization using the Faraday effect. *Opt. Lett.* **36**, 64–66 (2011). https://doi.org/10.1364/OL.36.000064

[61] Walpole, J. N. Semiconductor amplifiers and lasers with tapered gain regions. *Opt. Quant. Electron.* **28**, 623–645 (1996). https://doi.org/10.1007/BF00411298

[62] Jechow, A. *et al*. 1 W tunable near diffraction limited light from a broad area laser diode in an external cavity with a line width of 1.7 MHz. *Opt. Commun.* **277**, 161–165 (2007). https://doi.org/10.1016/j.optcom.2007.05.003

[63] Bayram, S. B. & Coons, R. W. Operation of a frequency-narrowed high-beam quality broad-area laser by a passively stabilized external cavity technique. *Rev. Sci. Instrum.* **78**, 116103 (2007). https://doi.org/10.1063/1.2804015

[64] Sell, J. F., Miller, W., Wright, D., Zhdanov, B. V. & Knize, R. J. Frequency narrowing of a 25 W broad area diode laser. *Appl. Phys. Lett.* **94**, 051115 (2009). https://doi.org/10.1063/1.3079418

[65] Goyal, A. K., Gavrilovic, P. & Po, H. Stable single-frequency operation of a high-power external cavity tapered diode laser at 780 nm. *Appl. Phys. Lett.* **71**, 1296–1298 (1997). https://doi.org/10.1063/1.119876

[66] Wakita, A. & Sugiyama, K. Single-frequency external-cavity tapered diode laser in a double-ended cavity configuration. *Rev. Sci. Instrum.* **71**, 1–4 (2000). https://doi.org/10.1063/1.1150150

[67] Chi, M. *et al*. Tunable high-power narrow-linewidth semiconductor laser based on an external-cavity tapered amplifier. *Opt. Express* **13**, 10589–10596 (2005). https://doi.org/10.1364/OPEX.13.010589

[68] Voigt, D., Schilder, E. C., Spreeuw, R. J. C. & van Linden van den Heuvell, H. B. Characterization of a high-power tapered semiconductor amplifier system. *Appl. Phys. B* **72**, 279–284 (2001). https://doi.org/10.1007/s003400100513

[69] Lang, R. Injection locking properties of a semiconductor laser. *IEEE J. Quantum. Electron*. **18**, 976–983 (1982). https://doi.org/10.1109/JQE.1982.1071632

[70] Blin, S. *et al*. Phase and spectral properties of optically injected semiconductor lasers. *C. R. Phys.* **4**, 687–699 (2003). https://doi.org/10.1016/S1631-0705(03)00083-5

[71] Shvarchuck, I., Dieckmann, K., Zielonkowski, M. & Walraven, J. T. M. Broad-area diode-laser system for a rubidium Bose−Einstein condensation experiment. *Appl. Phys. B* **71**, 475–480 (2000). https://doi.org/10.1007/s003400000395

[72] Sasaki, K., Yoneyama, T., Nakamura, T., Sato, S. & Takeyama, A. Semiconductor laser based, injection locking maintaining broad linewidth generated by a direct current modulation of a master laser. *Rev. Sci. Instrum. 77*, 096107 (2006). https://doi.org/10.1063/1.2349595

[73] Wilson, A. C., Sharpe, J. C., McKenzie, C. R., Manson, P. J. & Warrington, D. M. Narrow-linewidth master-oscillator power amplifier based on a semiconductor tapered amplifier. *Appl. Opt.* **37**, 4871–4975 (1998). https://doi.org/10.1364/AO.37.004871

[74] Nyman, R. A. *et al*. Tapered-amplified antireflection-coated laser diodes for potassium and rubidium atomic-physics experiments. *Rev. Sci. Instrum*. **77**, 033105 (2006). https://doi.org/10.1063/1.2186809

[75] Xiong, Y., Murphy, S., Carlsten, J. L. & Repasky, K. Design and characteristics of a tapered amplifier diode system by seeding with continuous-wave and mode-locked external cavity diode laser. *Opt. Eng.* **45**, 124205 (2006). https://doi.org/10.1117/1.2404925

[76] Bolpasi, V. & von Klitzing, W. Double-pass tapered amplifier diode laser with an output power of 1 W for an injection power of only 200 μw. *Rev. Sci. Instrum.* **81**, 113108 (2010). https://doi.org/10.1063/1.3501966

[77] Kangara, J. C. B. *et al*. Design and construction of cost-effective tapered amplifier systems for laser cooling and trapping experiments. *Am. J. Phys.* **82**, 805–817 (2014). https://doi.org/10.1119/1.4867376

[78] Hawthorn, C. J. Weber, K. P. & Scholten, R. E. Littrow configuration tunable external cavity diode laser with fixed direction output beam. *Rev. Sci. Instrum*. **72**, 4477–4479 (2001). https://doi.org/10.1063/1.1419217

[79] Kowalski, K. DLC 300 Laser Controller. Operating Manual. *Institute of Physics PAS.* http://info.ifpan.edu.pl/ON-2/on22/MOT/current_controller.html (Accessed: 30th July 2021)

[80] Kowalski, K. LTC302 Temperature Controller. Operating Manual. *Institute of Physics PAS.* http://info.ifpan.edu.pl/ON-2/on22/MOT/temperature_controller.html (Accessed: 30th July 2021)

[81] Yashchuk, V. V., Budker, D. & Davis, J. R. Laser frequency stabilization using linear magneto-optics. *Rev. Sci. Instrum.* **71**, 341–346 (2000). https://doi.org/10.1063/1.1150205

[82] Beverini N., Maccioni, E., Marsili, P., Ruffini, A. & Sorrentino. F. Frequency stabilization of a diode laser on the Cs D2 resonance line by the Zeeman effect in a vapor cell. *Appl. Phys. B* **73**, 133–138 (2001). https://doi.org/10.1007/s003400100618

[83] Donley, E. A., Heavner, T. P., Levi, F., Tataw, M. O. & Jefferts, S. R. Double-pass acousto-optic modulator system. *Rev. Sci. Instrum.* **76**, 063112 (2005). https://doi.org/10.1063/1.1930095

[84] de Carlos-López, E., López, J. M., López, S., Espinosa, M. G. & Lizama, L. A. Note: Laser frequency shifting by using two novel triple-pass acousto-optic modulator configurations. *Rev. Sci. Instrum*. **83**, 116102 (2012). https://doi.org/10.1063/1.4758998

[85] Buchkremer, F. B. J., Dumke, R., Buggle, Ch., Birkl, G. & Termer, W. Low-cost setup for generation of 3 GHz frequency difference phase-locked laser light. *Rev. Sci. Instrum.* **71,** 3306–3308 (2000). https://doi.org/10.1063/1.1287633

[86] Yun, P., Tan, B., Deng, W. & Gu, S. High coherent bi-chromatic laser with gigahertz splitting produced by the high diffraction orders of acousto-optic modulator used for coherent population trapping experiments. *Rev. Sci. Instrum.* **82**, 123104 (2011). https://doi.org/10.1063/1.3665986

[87] Gunawardena, M., Hess, P., W. Strait, J. & Majumder, P. K. A frequency stabilization technique for diode lasers based on frequency-shifted beams from an acousto-optic modulator. *Rev. Sci. Instrum.* **79**, 103110 (2008). https://doi.org/10.1063/1.3006386

[88] Liu, Z. & Slavik, R., Optical injection locking: from principle to applications. *J. Lightw. Technol.* **38**, 43–59 (2020). https://doi.org/10.1109/JLT.2019.2945718

[89] Lau, E. K., Wong, L. J. & Wu, M. C. Enhanced modulation characteristics of optical injection-locked lasers: A tutorial. *IEEE J. Sel. Top. Quantum Electron.* **15**, 618–633 (2009). https://doi.org/10.1109/JSTQE.2009.2014779

[90] Vainio, M., Merimaa, M. & Nyholm, K. Modulation transfer characteristics of injection-locked diode lasers. *Opt. Commun.* **267**, 455–463 (2006). https://doi.org/10.1016/j.optcom.2006.06.054

[91] Gertsvolf, M. & Rosenbluh, M. Injection locking of a diode laser locked to a Zeeman frequency stabilized laser oscillator.

Opt. Commun. **170**, 269–274 (1999). https://doi.org/10.1016/S0030-4018(99)00470-8

[92] Smith, D. A. & Hughes, I. G. The role of hyperfine pumping in multilevel systems exhibiting saturated absorption. *Am. J. Phys.* **72**, 631 (2004). https://doi.org/10.1119/1.1652039

[93] Siddons, P., Adams, C. S., Ge, C. & Hughes, I. G Absolute absorption on rubidium D lines: comparison between theory and experiment. *J. Phys. B: At. Mol. Opt. Phys.* **41**, 155004 (2008). https://doi.org/10.1088/0953-4075/41/15/155004

[94] Haldar, M. K., Coetzee, J. C. & Gan, K. B. Optical frequency modulation and intensity modulation suppression in a master–slave semiconductor laser system with direct modulation of the master laser. *IEEE J. Quantum Electron.* **41**, 280–286 (2005). https://doi.org/10.1109/JQE.2004.841501

[95] Fragkos, A., Bogris, A., Syvridis, D. & Phelan, R. Amplitude noise limiting amplifier for phase encoded signals using injection locking in semiconductor lasers. *J. Lightw. Technol.* **30**, 764–771 (2012). https://doi.org/10.1109/JLT.2011.2178816

[96] Lin, P.-Y., Shiau, B.-W., Hsiao, Y.-F. & Chen, Y.-C. Creation of arbitrary spectra with an acousto-optic modulator and an injection-locked diode laser. *Rev. Sci. Instrum.* **82**, 083108 (2011). https://doi.org/10.1063/1.3626903

[97] Haverkamp, M., Kochem, G. & Boucke, K. Single mode fiber coupled tapered laser module with frequency stabilized spectrum. *Proc. SPIE* **6876**, 68761D1-11 (2008). https://doi.org/10.1117/12.764801

[98] Taskova, E., Gateva, S., Alipieva, E., Kowalski, K., Głódź, M. & Szonert, J. Nonlinear Faraday rotation for optical limitation. *Appl. Opt.* **43**, 4178–4181 (2004). https://doi.org/10.1364/AO.43.004178

[99] Deninger, A., Kraft, S., Lison, F. & Zimmermann, C. Rubidium spectroscopy with 778- to 780-nm distributed feedback laser diodes. *Proc. SPIE* **5722**, 5722–61 (2005). https://doi.org/10.1117/12.590386

[100] Wells, S. R., Miyabe, M. & Hasegawa, S. Design, construction, and characterization of a single unit external cavity diode laser coupled tapered amplifier system for atomic physics. *Opt. Laser Technol.* **126**, 106118 (2020). https://doi.org/10.1016/j.optlastec.2020.106118